Real-time simulations of nonequilibrium transport in the single-impurity Anderson model

F. Heidrich-Meisner,[1] A. E. Feiguin,[2,3] and E. Dagotto[4]
[1]*Institut für Theoretische Physik C, RWTH Aachen University, 52056 Aachen, Germany and JARA–Jülich Aachen Research Alliance, Forschungszentrum Jülich, 52425 Jülich, Germany*
[2]*Microsoft Project Q, University of California, Santa Barbara, California 93106, USA*
[3]*Condensed Matter Theory Center, University of Maryland, College Park, Maryland 20742, USA*
[4]*Materials Science and Technology Division, Oak Ridge National Laboratory, Oak Ridge, Tennessee 37831, USA and Department of Physics and Astronomy, University of Tennessee, Knoxville, Tennessee 37996, USA*
(Received 23 March 2009; revised manuscript received 5 June 2009; published 29 June 2009)

One of the main open problems in the field of transport in strongly interacting nanostructures is the understanding of currents beyond the linear response regime. In this work, we consider the single-impurity Anderson model and use the adaptive time-dependent density matrix renormalization group method to compute real-time currents out of equilibrium. We first focus on the particle-hole symmetric point where Kondo correlations are the strongest and then extend the study of the nonequilibrium transport to the mixed-valence regime. As a main result, we present accurate data for the current-voltage characteristics of this model.

DOI: 10.1103/PhysRevB.79.235336 PACS number(s): 73.63.Kv, 73.23.−b, 72.10.Fk, 72.15.Qm

I. INTRODUCTION

Experiments in strongly interacting nanostructures are often well described by relatively simple model Hamiltonians. In several cases, these models are integrable and can be solved exactly,[1] or they can be studied using powerful numerical methods, such as the numerical renormalization group (NRG).[2,3] These techniques have had enormous success in describing the equilibrium properties of these models. However, the understanding of open systems out of equilibrium remains an extremely challenging area of research. While recent studies have succeeded in calculating the current-voltage (*I-V*) characteristics of the interacting resonant level model,[4–8] the focus of current research has been devoted toward the more difficult single-impurity Anderson model incorporating Kondo correlations. For example, experimental results for the finite-bias transport properties of a quantum dot still await a complete theoretical explanation.[9–12] Besides the fundamental interest in solving this type of problems, Kondo physics is an emergent feature in many experiments on nanoscopic systems.[9–11]

Our goal here is to calculate the *I-V* characteristics of the single-impurity Anderson model, described by the Hamiltonian $H=H_{\rm dot}+H_{\rm leads}$ (Ref. 13):

$$H_{\rm dot} = V_{\rm g}\sum_{\sigma} n_{1\sigma} + U/2\sum_{\sigma} n_{1\sigma}n_{1\bar{\sigma}}$$

$$H_{\rm leads} = -t'\sum_{l=R,L;\sigma}(c^{\dagger}_{1,\sigma}c_{l,1,\sigma} + \text{H.c.}) - \sum_{n=1;l=R,L;\sigma}^{N_{L,R}} t_n(c^{\dagger}_{l,n,\sigma}c_{l,n+1,\sigma} + \text{H.c.}). \quad (1)$$

$H_{\rm dot}$ contains the gate potential $V_{\rm g}$ and the Coulomb repulsion U acting on the dot. The first term in $H_{\rm leads}$ is the hybridization of the dot with the conduction band, and the last term describes the leads. $N_{L(R)}$ is the number of sites on the left (right) lead, with $N=N_L+N_R+1$. $c^{\dagger}_{\nu,\sigma}$ is a fermionic creation operator acting on the dot ($\nu=1$) or a site i in the left (right) lead [$\nu=L(R),i$], with a spin index $\sigma=\uparrow,\downarrow$.

The Kondo resonance is a signature of the hybridization of the leads with a single electron on the dot.[13] Electrons from the leads screen the extra spin, forming an overall singlet, and the corresponding Kondo cloud.[13] This collective state can be suppressed, and eventually destroyed, by temperature, magnetic field, or a large bias between the leads. The ultimate goal is to understand the subtle mechanisms behind the suppression of the Kondo resonance, and how this response translates into the *I-V* characteristics of the system. In particular, when a finite voltage bias is applied, results for the density of states (DOS) at the particle-hole symmetric point $V_{\rm g}=-U/2$ seem to indicate[14–18] that the Kondo peak smoothly decreases, while the spectral weight is transferred to satellite peaks centered at the chemical potentials of the leads at frequencies $\omega\approx\pm V/2$. At large biases, these peaks merge with broad shoulders at $\omega\approx\pm U/2$.[14–18] The possible existence of a negative differential conductance in the high-voltage regime of nanostructures is a topic of intense discussion.[4]

Beyond perturbative limits in U or bias voltage V, the properties of the steady state, including average currents, are still under scrutiny. Therefore, to gauge the validity of approximate analytical schemes used to study nonequilibrium transport, it is highly desirable to have accurate numerical results available as a benchmark. Several efforts to work out the nonlinear transport regime of this model have been made using perturbative[14,19,20] as well as renormalization schemes,[21–26] the noncrossing approximation,[17,18] flow equations,[27] real-time path integral approaches,[28] quantum Monte Carlo (QMC),[15,29,30] and the Bethe ansatz.[31] Recently, the time-dependent NRG method has been used to simulate aspects of nonequilibrium physics in quantum dots.[16,32–34] In this work, we introduce the time-dependent density matrix renormalization group (tDMRG)[35,36] to address two questions: first, what is the *I-V* characteristics at $V_{\rm g}=-U/2$ and, second, how do nonequilibrium currents behave in the mixed-valence regime. Furthermore, tDMRG gives access to the transient regime, i.e., information on how the steady state is reached, which some of the aforementioned methods are,

as of now, not designed for. We will also provide a technical discussion of our tDMRG calculations, in terms of system sizes and accuracy needed to obtain high quality results. We work at values of $U/\Gamma \leq 8$, where $\Gamma = 2\pi\rho_{\text{leads}}(E_F)t'^2 = 2t'^2$ is the hybridization parameter, with $\rho_{\text{leads}}(E_F)$ the density of states in the tight-binding leads at the Fermi energy E_F. Our approach employs a real-space representation of the leads with $t_n = 1$, which we find is a useful modeling of the leads for bias values $V \gtrsim T_K$, where T_K is the Kondo temperature. In the case of $V_g = -U/2$, our results are in excellent agreement with those from the functional renormalization group (fRG)[22] for $U/\Gamma \leq 8$.

The plan of this exposition is the following. In Sec. II, we shall introduce our numerical approach, the tDMRG, and we discuss the error sources and the quality of our numerical data. In Sec. III, we present our results for the particle hole-symmetric point, while in Sec. IV, we turn to the mixed-valence regime. We conclude with a summary and discussion of our results in Sec. V.

II. NUMERICAL METHOD: DMRG

The tDMRG method has previously been used in Refs. 37 and 38 to study the linear conductance of the single-impurity Anderson model Eq. (1). In the latter effort, it has been argued that a logarithmic discretization,[3] i.e., $t_n \propto \lambda^{-n/2}$ is useful in capturing Kondo correlations in the linear conductance at $V_g = -U/2$ and using this trick, perfect conductance was obtained for $U/\Gamma \lesssim 7$. Other applications of the tDMRG to transport in nanostructures include the (interacting) resonant level model,[4,39] short chains of spinless fermions[40,41] as well as nonequilibrium transport through a point contact in a non-Abelian quantum Hall state.[42] Moreover, first tDMRG results for Eq. (1) out of equilibrium and at $V_g = -U/2$ were presented in Ref. 43 by Kirino *et al.* for $U/\Gamma \leq 2.8$ and in Ref. 38 for $U/\Gamma = 3.125$. We here move substantially beyond the scope of these previous studies[38,43] as we consider larger values of U/Γ, perform a finite-size scaling analysis, and use up to $m = 2000$ DMRG states during the time-evolution (compared to $m = 800$ in Ref. 43).

In our numerical calculations,[37,38] we first compute the ground state of Eq. (1) and then, at time $\tau = 0^+$, we apply an extra term H_{bias} and evolve under $H + H_{\text{bias}}$:

$$H_{\text{bias}} = \frac{V}{2}\sum_{n=1}^{N_R} n_{R,n} - \frac{V}{2}\sum_{n=1}^{N_L} n_{L,n}. \tag{2}$$

Here, $n_{R(L),n} = \Sigma_\sigma c^\dagger_{R(L),n,\sigma} c_{R(L),n,\sigma}$. In principle, different spatial forms of V can be used,[35,40] which sometimes affect the transient behavior but leave the steady-state currents unchanged. We measure the expectation value $J(\tau)$ of the local current operator acting on the links connecting the dot to the leads, averaging over the right and left links.[37,38] We set $e = \hbar = 1$. All simulations are performed at an overall half filling of dot and leads.

In our tDMRG runs, we use a Trotter-Suzuki time evolution scheme with time-steps of $0.05 \leq \delta\tau t \leq 0.15$. We find a fast convergence with system size on chains with $N_L(N_R)$ odd (even).[37,44] Our goal is to achieve a numerical accuracy of $\delta J_{\text{steady}}/V \sim 0.01 G_0$, where G_0 is the conductance quantum. The steady-state currents are computed by taking suitable time-averages, i.e., $J_{\text{steady}} = \langle J \rangle_\tau$. In principle, the true steady state is only reached for $N \to \infty$, while on finite systems, the term quasi-steady states may be more appropriate. For simplicity, we do not make this distinction here.

The error sources in tDMRG are:[38,45] (i) truncation errors, (ii) the Trotter error, and (iii) the determination of the time intervals to extract average currents from the real-time data at a given bias. Typically, we perform runs with different discarded weights $\delta\rho$ at fixed U, Γ, V, and N to identify the time windows for the averaging. We find (i) and (iii) to be the dominant sources in the present problem as the Trotter errors can effectively be reduced by using small time-steps and this error grows only linearly with the simulation time.[46] The truncation errors can be suppressed by decreasing the discarded weight $\delta\rho$ (Ref. 46) during the time evolution. This error source is thus well controlled, too. As for the averaging procedure, the determination of steady-state regimes are the least unambiguous for large gate voltages, intermediate biases voltages $V \gtrsim T_K$, and/or large $U/\Gamma \gtrsim 6$. There, the accuracy of our data for $\langle J \rangle_\tau / V$ is worse than $0.01 G_0$.

An important aspect of any simulation of time-evolution is the entanglement growth (see, e.g., Ref. 47). This is measured through the entanglement entropy $S_l = -\text{tr}(\rho_l \ln(\rho_l))$, where ρ_l is the reduced density matrix for a block of length l, as is naturally accessed in DMRG.[46] As our setup realizes a so-called global quantum quench, S_l can grow significantly as a function of time. As a consequence, to keep the truncated weight below a given threshold, an increasing number of states needs to be kept during the time evolution. For $V \gtrsim 0.1t$, it is imperative to work at a fixed $\delta\rho$ (as compared to a fixed m) during the time evolution to have first, an efficient simulation and second, a meaningful control over the numerical accuracy by studying the scaling in $\delta\rho$. Typically, to meet our target accuracy at $V \leq 2t$, a discarded weight of $\delta\rho \lesssim 10^{-7}$ is found to be appropriate.

III. RESULTS FOR PARTICLE-HOLE SYMMETRY

After these remarks on the method, we turn to the discussion of our tDMRG results. The time-dependent currents at $V_g = -U/2$ are displayed in Fig. 1 for $U/\Gamma = 2$ ($U = 0.5t$) and $V/U = 0.4, 0.6, \ldots, 2.0$. Since we plot $J(\tau)/V$, the currents decrease as the bias increases. An example for the time-interval used to compute the steady-state currents is indicated by arrows for the case of $V = 1.2U$ in the figure. While a full analysis of the short-time transients and its dependence on both V and Γ (see also Ref. 48) will be presented elsewhere, note that the transient time, i.e., the time for the current to reach its steady-state plateau, *decreases* as the bias increases, to, e.g., about $\tau \sim 6/t$ at $V \gtrsim 2U$ and $U = t/2$. This is illustrated in the inset of Fig. 1, where we estimate the transient time from the time that it takes the initial maximum in $J(\tau)$ to decay. For this reason, and due to less severe finite-size effects, short chains of $N \sim 24, 32, 48$ are often sufficient at large biases.

The average currents $\langle J \rangle_\tau$ are plotted as a function of bias in Fig. 2(a) for $U/\Gamma = 2, 4, 6$ ($U = 0.5t$ for all three sets, plus

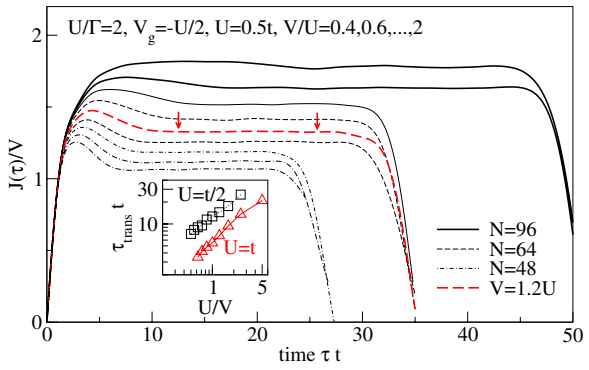

FIG. 1. (Color online) Particle-hole symmetric point, $V_g=-U/2$: Current $J(\tau)/V$ vs time τ for $U/\Gamma=2$ ($U=0.5t$, $t'=0.3535t$, $V_g=-U/2$) for $V/U=0.4,0.6,\ldots,2$ [$N=96$ (thick lines); $N=64$ (dashed lines); $N=48$ (dot-dashed lines)]. The arrows indicate the time-interval used for the calculation of the steady-state current $J_{\text{steady}}=\langle J(\tau)\rangle_\tau$ for $V/U=1.2$ from a time average $\langle\cdot\rangle_\tau$ (Ref. 38). Inset: estimates of the transient time τ_{trans} as a function of bias for $U=t/2$ (squares, $\Gamma=t/4$) and $U/t=1$ (triangles up, $\Gamma=t/2$), both at $U/\Gamma=2$.

additional $U=t$ curves for $U/\Gamma=2$ and 8). For $U/\Gamma=2$ and $U=t$, the average current increases monotonically with bias and eventually decreases. The latter gives rise to a negative differential conductance, yet this is simply due to the decreasing overlap of the leads' DOS, which have a finite bandwidth of $4t$ in our case. For that reason, namely the finite bandwidth, the current vanishes in the limit of $V\to\infty$ in our simulations.

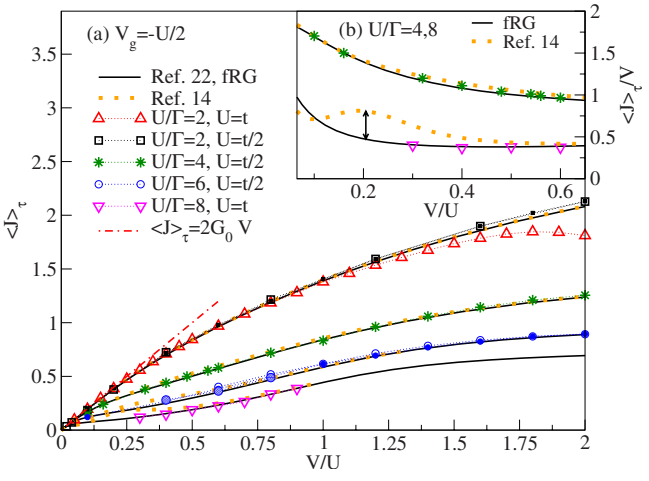

FIG. 2. (Color online) Particle-hole symmetric point, $V_g=-U/2$: (a) Current-voltage curves for $U/\Gamma=2,4,6$ with $U=t/2$ (squares, stars, circles) as well as data for $U/\Gamma=2,8$ with $U=t$ (triangles down and up, respectively). Open symbols: $N=64$, full ones: $N=96$ sites, shaded ones: $N=128$, stars and triangles down: finite-size extrapolations in $1/N$ ($U/\Gamma=4,8$ only). Dash-dotted line: $\langle J\rangle_\tau=2G_0V$. (b) Enlarged view of the low-bias region for $U/\Gamma=4$ and 8, $\langle J\rangle_\tau/V$ vs. V. Solid lines: fRG results from Ref. 22; dotted lines: 4th-order perturbation theory results from Ref. 14. (from top to bottom). For $U/\Gamma=8$, the arrow in the inset indicates the difference between the fRG and tDMRG results on the one hand and those from Ref. 14 on the other hand. For NRG results for T_K, see, e.g., Fig. 6 in Ref. 38.

We can estimate at which voltage the band-curvature and the finite bandwidth, and thus the deviation from the wide-band limit, start to play a role by varying U while keeping U/Γ fixed. Comparing $U=0.5t$ (squares) and $U=t$ (triangles up) results in Fig. 2(a) at $U/\Gamma=2$, we find that the smaller Us give the best agreement with fRG[22] (thick, solid lines) at large voltages. Note that the fRG calculations at these small values of $U/\Gamma\sim 2$ are expected to be very reliable. We thus mostly use $U=0.5t$ for our runs at larger values of U/Γ as we can then compare to the fRG at larger values of V. This has the disadvantage that the transient time increases with increasing $1/\Gamma$ (corresponding to a decreasing U at a fixed U/Γ; see the inset of Fig. 1), and therefore, for the runs at $U/\Gamma=8$ where we are interested in the behavior at intermediate bias values, we use $U=t$.

At $U/\Gamma=6$, a tendency of separating the narrow Kondo peak at small bias values from the Coulomb blockade peak at $V/U\gtrsim 0.5$ is visible. Unfortunately, at biases $V\sim 0.2U$, we observe a crossover in the monotonic behavior of our finite-size data, with $\langle J\rangle_\tau$ increasing (decreasing) with system size at small (large) biases.[38] This renders this bias regime the most difficult for the determination of steady-state regimes.

We emphasize the excellent agreement with the fRG results,[22] in particular, for bias voltages $V>T_K$. The differences between tDMRG and fRG seen at larger biases for the $U=t$ curve are due to the wide-band limit taken in fRG with a flat DOS (linear dispersion), compared to a semielliptical DOS in tDMRG calculations, as discussed above. We further compare to the 4th-order perturbation theory results (Ref. 14; dotted lines in Fig. 2). While overall, the three methods agree for $V>T_K$ and $U/\Gamma=2$, the perturbation theory result lies slightly above both tDMRG and fRG for $U/\Gamma=4$ and in the interval $0.2U\lesssim V\lesssim 0.8U$ [see Fig. 2(b)]. Note, though, that the differences between fRG and Ref. 14 are, at $U/\Gamma=4$, rather small and difficult to resolve numerically, but become more significant at $U/\Gamma=6$ and 8.

Therefore, we also consider the behavior for $U/\Gamma=8$ and $0.3\lesssim V/U\lesssim 0.9$, for which the accuracy of our data is reduced to $\delta\langle J\rangle_\tau/V\approx 0.03G_0$, due to an additional oscillatory component in the transient behavior that becomes more prominent at large U/Γ.[48] Nevertheless, as Fig. 2(b) clearly shows, our tDMRG results are still in good agreement with fRG, while the corresponding 4th-order perturbation theory[49] predicts too high values of $\langle J\rangle_\tau/V$. This constitutes an example where our numerical results serve to support the validity of one analytical approach, the fRG in this case, while unveiling that 4th-order perturbation theory[14] seems to break down at $U/\Gamma\gtrsim 6$ [see Fig. 2(b)]. Consequently, we may conclude that the double-minimum structure that Ref. 14 predicts to exist in the differential conductance likely is an artifact of approximations. This double minimum is precisely seen in the bias window in which the differences between our tDMRG and the 4th-order perturbation theory are the largest.

As for the regime $V\lesssim T_K$, note that at $V/U=0.1$ and $U/\Gamma=2$, the $N=96$ result reaches about 99% of the expected perfect conductance. At larger U/Γ and $V\lesssim 0.2U$, the currents from $N\lesssim 128$ are below the fRG result. Yet, for $U/\Gamma=4$ and, e.g., $V/U=0.1$ and 0.16, we have extrapolated the finite-size data for $\langle J\rangle_\tau/V$ in $1/N$ [see Fig. 2(b)]. The agreement with fRG is quite reasonable.

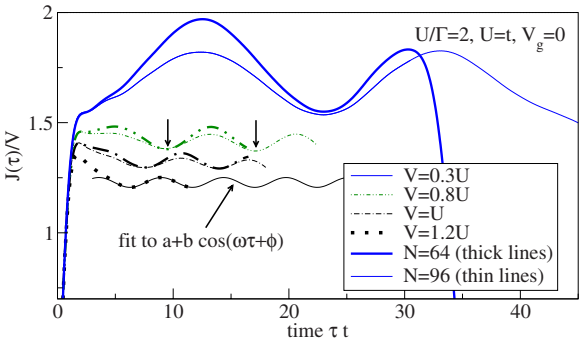

FIG. 3. (Color online) Mixed-valence regime: Current $J(\tau)/V$ vs time τ for $U/\Gamma=2$ ($U=t$, $t'=0.5t$, $V_g=0$ and bias values $V/U=0.3,0.8,1,1.2$ [$N=96$ (thin lines), $N=64$ (thick lines)]. Arrows indicate the interval used for the averaging for $\Delta V=0.8U$ and $N=64$. The thin solid line for $V=1.2U$ is a fit of $a+b\cos(\omega\tau+\phi)$ to the corresponding $N=64$ tDMRG data (dotted line).

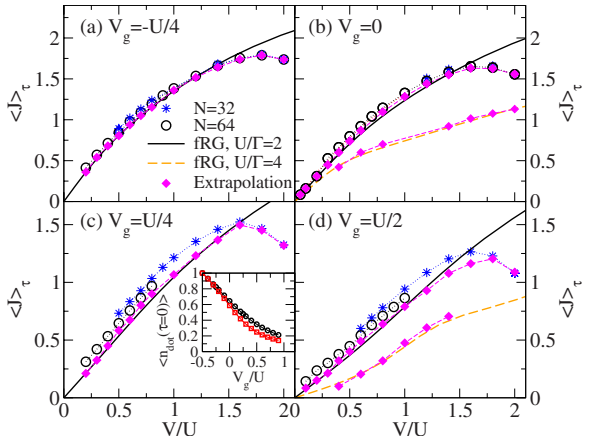

FIG. 4. (Color online) Mixed-valence regime: Current-voltage curves for $U/\Gamma=2$ ($U=t$, symbols with dotted lines), $U/\Gamma=4$ [$U=t/2$, extrapolated data only, panels (b) and (d)], and several gate potentials: (a) $V_g=-U/4$; (b) $V_g=0$; (c) $V_g=U/4$; and (d) $V_g=U/2$. Solid diamonds are extrapolations of finite-size data in $1/N$. Inset in (c): $\langle n_{dot}(\tau=0)\rangle$ vs V_g/U for $U/\Gamma=2$ (circles) and 4 (squares).

IV. RESULTS FOR THE MIXED-VALENCE REGIME

We now turn our attention to the mixed-valence regime $V_g \neq -U/2$, concentrating on $U/\Gamma=2$ and 4. Real-time currents are shown in Fig. 3 for $U/\Gamma=2$ ($U=t$) and $V_g=0$. In contrast to the $V_g=-U/2$ case, significant oscillations with a period $T\propto 1/V$ (Ref. 48) in the current are observed. These are due to finite-size gaps and their amplitudes decay with $1/N$. In principle, similar oscillations can be seen in the particle-hole symmetric case in the two local currents connecting the dot to the left and right lead. As in computing $\langle J\rangle_\tau$, we average over these two local currents and as they oscillate with a phase shift of π,[40] the oscillations cancel out in $\langle J\rangle_\tau$ at $V_g=-U/2$, but not away from that special point. For a detailed discussion of such oscillations in tDMRG calculations of real-time currents, see Ref. 40. We exploit the existence of these oscillations to determine intervals to compute steady-state currents from,[40] averaging over a full period (see the arrows in Fig. 3 and the fit to the $V=1.2U$ data for an illustration).

The average currents $\langle J\rangle_\tau$ are plotted vs bias in Fig. 4 for $U/\Gamma=2$ and 4. For $U/\Gamma=2$, we include the results from system sizes of $N=32$ and $N=64$ sites to illustrate the emergent finite-size effects. To our advantage, we find that at large biases, even small chains of 32 sites yield well-converged results, as the example of $V_g=-U/4$ and $U/\Gamma=2$ shows [see Fig. 4(a)]. Although we have not pursued this, it is reasonable to expect that at bias values of $V/U\gtrsim 2$, exact diagonalization may produce useful results as well.

For several values of the bias, we have extrapolated the average currents in $1/N$ (shown as solid diamonds in Fig. 4). As compared to the $V_g=-U/2$ case, finite-size effects are somewhat more significant, as in our setup, the average filling of the leads slightly exceeds hall filling whenever $V_g \neq -U/2$. The figure further includes the respective fRG results,[22] with a very good agreement with our extrapolated data. Slight deviations between fRG and tDMRG at intermediate bias voltages can be attributed to: (i) uncertainties in the extrapolation of the finite-size data and (ii) the curvature of the bands. Note that the band effects already yield small differences in the linear conductance as obtained from tDMRG when compared to results valid in the wide-band (linear dispersion) limit (see, e.g., Fig. 13 in Ref. 37).

V. SUMMARY

In this work, we carried out large scale and accurate time-dependent simulations using the adaptive tDMRG method to study transport in the single-impurity Anderson model at large biases. By performing a finite-size analysis with chains of up to $N=128$ sites, we were able to compute the current-voltage characteristics at the particle-hole symmetric point up to $U/\Gamma=8$. Convergence with system size is very fast in the voltage regime $T_K \lesssim V \lesssim 2t$, while the resolution in the Kondo regime, i.e., $V \lesssim T_K$, is hampered by finite-size effects, due to the exponentially large Kondo correlations[13] (see Ref. 38, though). Our results are in excellent agreement with those from fRG[22] for $U/\Gamma \lesssim 8$, lending strong support to the validity of both approaches. Where converged, our data thus provide an unbiased benchmark from a quasiexact method for analytical or approximate numerical approaches. Furthermore, we studied the mixed-valence regime by varying the gate potential at fixed U/Γ, presenting results for current-voltage characteristics.

Let us conclude by comparing our numerical approach, the tDMRG, to other numerical methods recently applied to nonequilibrium transport in the single-impurity model, namely, real-time QMC simulations, and the real-time NRG. A direct comparison of our results with the QMC data of Ref. 29 (not shown here) reveals a reasonably good agreement at large bias voltages $V>T_K$. At small bias voltages, the QMC data are consistently below both tDMRG and fRG. This can be traced back to the fact that, due to the sign problem, QMC simulations are limited to short time scales with a maximum time on the order of $3/\Gamma$,[29] while in our case, we are able to reliably simulate times on the order of $\tau \lesssim 6/\Gamma$ at large biases $V\sim t$ and $\tau \lesssim 12/\Gamma$ at small biases

$V \sim 0.2t$ (compare Fig. 1). We should emphasize, though, that the QMC simulations in the strong-coupling case start from the dot being decoupled from the leads in the initial state, which is different from our initial condition and which may lead to a transient behavior different from our case. An advantage of the real-time QMC[29,30] is that it is designed for the thermodynamic limit, yet we have shown here that a finite-size analysis of tDMRG yields very accurate results. Within both methods, the transient regime, i.e., the time window between the initial state and the steady-state regime can be studied.[50]

Time-dependent NRG results were published for the differential conductance δG and large ratios of U/Γ (Ref. 16). One the one hand, one may generally expect time-dependent NRG to be well suited to capture the finite-bias behavior in the Kondo regime $V \lesssim T_k$, while on the other hand, the data presented for δG at discrete bias voltages, seem to be somewhat noisy at large and intermediate biases [see Fig. 3(c) in Ref. 16], rendering a comparison with our data difficult. Real-time NRG calculates the steady-state density operator and then extracts the current and the nonequilibrium spectral density from that information. The numerical challenges in obtaining accurate data for steady-state currents seem to be (a) keeping a sufficiently large number of states and (b) artifacts due to the logarithmic discretization.[16] Real-time NRG simulations can be performed at finite temperatures as well,[16] while methods for real-time DMRG simulations at finite temperatures are under development[51–54] and may be available for the study of nonequilibrium currents in the near future.

Our work establishes an important application of the adaptive tDMRG to a topic of much interest to both experimentalists and theoretical researchers. As the technique is highly flexible and can easily be adapted to impurity problems beyond Eq. (1) such as interacting leads[42] or complex geometries, we are convinced that this tool will become highly instrumental in future studies of nonequilibrium transport in nanoscopic systems.

ACKNOWLEDGMENTS

We acknowledge valuable discussions with N. Andrei, L. Dias da Silva, S. Jakobs, V. Meden, H. Onishi, M. Pletyukhov, G. Roux, H. Schoeller, and P. Werner. We further thank the authors of Ref. 22 for sending us their results for comparison. E.D. was supported in part by the NSF under Grant No. DMR-0706020 and the Division of Materials Science and Engineering, U.S. DOE, under contract with UT-Battelle, LLC. F.H.-M. acknowledges support by the DFG through FOR 912 under Grant No. HE 5242/2-1. A.E.F. was supported by Microsoft Station Q.

[1] N. Andrei, Phys. Rev. Lett. **45**, 379 (1980).
[2] K. G. Wilson, Rev. Mod. Phys. **47**, 773 (1975).
[3] R. Bulla, T. Costi, and T. Pruschke, Rev. Mod. Phys. **80**, 395 (2008).
[4] E. Boulat, H. Saleur, and P. Schmitteckert, Phys. Rev. Lett. **101**, 140601 (2008).
[5] P. Mehta and N. Andrei, Phys. Rev. Lett. **96**, 216802 (2006).
[6] B. Doyon, Phys. Rev. Lett. **99**, 076806 (2007).
[7] L. Borda, K. Vladár, and A. Zawadowski, Phys. Rev. B **75**, 125107 (2007).
[8] A. Nishino, T. Imamura, and N. Hatano, Phys. Rev. Lett. **102**, 146803 (2009).
[9] D. Goldhaber-Gordon, H. Shtrikman, D. Mahalu, D. Abusch-Magder, U. Meirav, and M. A. Kastner, Nature (London) **391**, 156 (1998).
[10] W. G. van der Wiel, S. D. Franceschi, T. Fujisawa, J. M. Elzerman, S. Tarucha, and L. P. Kouwenhoven, Science **289**, 2105 (2000).
[11] M. Grobis, I. G. Rau, R. M. Potok, H. Shtrikman, and D. Goldhaber-Gordon, Phys. Rev. Lett. **100**, 246601 (2008).
[12] G. D. Scott, Z. K. Keane, J. W. Ciszek, J. M. Tour, and D. Natelson, Phys. Rev. B **79**, 165413 (2009).
[13] A. Hewson, *The Kondo Problem to Heavy Fermions* (Cambridge University Press, Cambridge, UK, 1993).
[14] T. Fujii and K. Ueda, Phys. Rev. B **68**, 155310 (2003).
[15] J. E. Han and R. J. Heary, Phys. Rev. Lett. **99**, 236808 (2007).
[16] F. B. Anders, Phys. Rev. Lett. **101**, 066804 (2008).
[17] Y. Meir, N. S. Wingreen, and P. A. Lee, Phys. Rev. Lett. **70**, 2601 (1993).
[18] N. S. Wingreen and Y. Meir, Phys. Rev. B **49**, 11040 (1994).
[19] S. Hershfield, J. H. Davies, and J. W. Wilkins, Phys. Rev. Lett. **67**, 3720 (1991).
[20] S. Hershfield, J. H. Davies, and J. W. Wilkins, Phys. Rev. B **46**, 7046 (1992).
[21] B. Doyon and N. Andrei, Phys. Rev. B **73**, 245326 (2006).
[22] S. Jakobs, M. Pletyukhov, and H. Schoeller (unpublished).
[23] H. Schoeller and J. König, Phys. Rev. Lett. **84**, 3686 (2000).
[24] A. Rosch, J. Kroha, and P. Wölfle, Phys. Rev. Lett. **87**, 156802 (2001).
[25] R. Gezzi, T. Pruschke, and V. Meden, Phys. Rev. B **75**, 045324 (2007).
[26] S. G. Jakobs, V. Meden, and H. Schoeller, Phys. Rev. Lett. **99**, 150603 (2007).
[27] S. Kehrein, Phys. Rev. Lett. **95**, 056602 (2005).
[28] S. Weiss, J. Eckel, M. Thorwart, and R. Egger, Phys. Rev. B **77**, 195316 (2008).
[29] P. Werner, T. Oka, and A. J. Millis, Phys. Rev. B **79**, 035320 (2009).
[30] M. Schiró and M. Fabrizio, Phys. Rev. B **79**, 153302 (2009).
[31] R. M. Konik, H. Saleur, and A. W. W. Ludwig, Phys. Rev. Lett. **87**, 236801 (2001).
[32] F. B. Anders and A. Schiller, Phys. Rev. Lett. **95**, 196801 (2005).
[33] F. B. Anders and A. Schiller, Phys. Rev. B **74**, 245113 (2006).
[34] D. Roosen, M. R. Wegewijs, and W. Hofstetter, Phys. Rev. Lett. **100**, 087201 (2008).
[35] S. R. White and A. E. Feiguin, Phys. Rev. Lett. **93**, 076401 (2004).

[36] A. Daley, C. Kollath, U. Schollwöck, and G. Vidal, J. Stat. Mech.: Theory Exp. (2004) P04005.
[37] K. A. Al-Hassanieh, A. E. Feiguin, J. A. Riera, C. A. Büsser, and E. Dagotto, Phys. Rev. B **73**, 195304 (2006).
[38] L. G. G. V. Dias da Silva, F. Heidrich-Meisner, A. E. Feiguin, C. A. Büsser, G. B. Martins, E. V. Anda, and E. Dagotto, Phys. Rev. B **78**, 195317 (2008).
[39] C. Guo, A. Weichselbaum, S. Kehrein, T. Xiang, and J. von Delft, Phys. Rev. B **79**, 115137 (2009).
[40] G. Schneider and P. Schmitteckert, arXiv:cond-mat/0601389 (unpublished).
[41] P. Schmitteckert, Phys. Rev. B. **70**, 121302(R) (2004).
[42] A. Feiguin, P. Fendley, M. P. A. Fisher, and C. Nayak, Phys. Rev. Lett. **101**, 236801 (2008).
[43] S. Kirino, T. Fujii, J. Zhao, and K. Ueda, J. Phys. Soc. Jpn. **77**, 084704 (2008).
[44] F. Heidrich-Meisner, G. B. Martins, C. A. Büsser, K. A. Al-Hassanieh, A. E. Feiguin, G. Chiappe, E. V. Anda, and E. Dagotto, Eur. Phys. J. B **67**, 527 (2009).
[45] D. Gobert, C. Kollath, U. Schollwöck, and G. Schütz, Phys. Rev. E **71**, 036102 (2005).
[46] U. Schollwöck, Rev. Mod. Phys. **77**, 259 (2005).
[47] P. Calabrese and J. Cardy, J. Stat. Mech.: Theory Exp. (2007) P06008.
[48] A. Schiller and S. Hershfield, Phys. Rev. B **62**, R16271 (2000).
[49] The 4th-order perturbation theory data are taken from the preprint version of Ref. 14; T. Fujii and K. Ueda, arXiv:cond-mat/0211616v1.
[50] T. L. Schmidt, P. Werner, L. Mühlbacher, and A. Komnik, Phys. Rev. B **78**, 235110 (2008).
[51] F. Verstraete, J. J. García-Ripoll, and J. I. Cirac, Phys. Rev. Lett. **93**, 207204 (2004).
[52] A. E. Feiguin and S. R. White, Phys. Rev. B **72**, 220401(R) (2005).
[53] T. Barthel, U. Schollwöck, and S. R. White, Phys. Rev. B **79**, 245101 (2009).
[54] J. Sirker and A. Klümper, Phys. Rev. B **71**, 241101(R) (2005).